Chapter 2

Single crystal growth and characterization tools

A high-quality single crystal is required to witness the distinctive quantum phenomena connected to the electronic structure. Because it is exceedingly challenging to see the exciting quantum effects in the lab without a perfect single crystal, a flawless single crystal growth technique is crucial. This chapter discusses the specific synthesis process that was utilized to prepare the sample as well as the operation of the various characterization techniques that were employed in this thesis work to characterize various sample attributes.

2.1 Single crystal growth technique

In the field of materials science, a single crystal is a type of material in which the crystal lattice of the entire sample is continuous and unbroken all the way, and there are no grain boundaries. Other names for this type of material include single-crystal solid or monocrystalline solid. The absence of the defects that are associated with grain boundaries can give monocrystals distinctive capabilities, in particular those that are mechanical, optical, and electrical. These characteristics, which can also be anisotropic, can vary depending on the type of crystallographic structure. Because of these characteristics, certain gemstones are valued highly and are also put to use in a variety of technological applications, par-

Figure 2.1: The naturally grown large quartz crystal (The photo is taken from the official website of the natural history museum of Bern[33])

ticularly in the fields of optics and electronics. Perfect single crystals of relevant size are extremely uncommon in nature. This is because entropic processes favour the presence of certain faults in the microstructure of solids, such as impurities, inhomogeneous strain, and crystallographic defects like as dislocations. In many cases, the requisite laboratory conditions contribute to an increase in production costs. On the other hand, defective single crystals have the potential to grow to gigantic sizes in nature. It is known that several different types of minerals, including beryl, feldspars and gypsum, have created crystals that are several metres across (The naturally grown crystal are shown as an example in Fig. 2.1)

Crystals can be artificially grown from a melt, solid, vapour, or solution. The Czochralski process (CZ), the Floating zone technique (also known as Zone Movement), and the Bridgman technique are all examples of specific methods that can be used to manufacture enormous single crystals, sometimes known as boules. The first people to employ the Czochralski process to make Ge and Si single crystals worked at Bell Telephone Laboratories. Dr. Teal and Dr. Little were the pioneers of this technique. Crystallisation can also be

accomplished via hydrothermal synthesis, sublimation, or even just crystallisation in the presence of a solvent, depending on the various physical qualities of the substance being crystallised. A modified version of the Kyropoulos method, for instance, can be applied to the cultivation of high-quality sapphire single crystals weighing 300 kilogrammes. Prior to the development of CZ, rubies were traditionally produced using a technique known as the Verneuil process, which is also known as the flame-fusion method. There have been recent developments in the field, such as chemical vapour depositions (CVD), as well as a variety of new variations and improvements to the technologies that are already in use. The diagram does not include these elements. In order to grow single crystals in our laboratory facility, we primarily make use of the chemical vapour transport (CVT), flux, and Bridgeman techniques.

2.1.1 CVT method

Chemical vapour transport, or CVT for short, is a technique that was made popular by Schäfer. CVT is a process in which a condensed phase, often a solid, is volatilized in the presence of a gaseous reactant (transport agent), and the resulting crystals are deposited in another location. Halogens and compounds of halogens are examples of common types of transport agents. The apparatus comprises of a furnace with two distinct temperature zones (source T2 and sink T1), an ampoule containing both the reactant and the transport agent, and the ampoule itself. The growth temperature, the transport direction, the rate of the mass transport, the choice of the transport agent, and the free energy of the reaction are the numerous parameters that need to be adjusted for a successful CVT. Convection and diffusion are the underlying mechanisms that determine how things move. In spite of the fact that increasing the transport rates that favour convection can result in the formation of larger crystals, the resulting crystals are inhomogeneous and more prone to having flaws. As a result, optimisation of each chemical system is absolutely necessary. Both the source temperature and the sink temperature need to be adjusted, depending on the free energy released during the reaction between the species. A movement from a cold zone to a hot zone is indicated by a reaction that is exothermic, whereas the opposite is anticipated for a

reaction that is endothermic. Furthermore, no transport occurs if the interspecies reaction is very exothermic or very endothermic.

2.1.2 Flux method

Crystals can be grown using a technique known as the flux method, which involves dissolving the constituents of the desired chemical in a liquid known as flux. Crystals that must be free from thermal strain are a good candidate for the approach because it is particularly suitable for them. The process is carried out inside a crucible that is constructed from a substance that is extremely stable and does not react. Metals such as platinum, tantalum, and niobium are frequently utilised in the manufacturing process of oxide crystals. Crucibles typically constructed from ceramic materials including alumina, zirconia, and boron nitride are used in the production of metallic crystals. When conducting a reaction, it is common practise to encapsulate the crucibles and their contents in a quartz ampoule or use a furnace that has an environment control feature in order to keep them protected from the air. To make a saturated solution, you must first build a full solution by holding the constituents of the desired crystal and the flux at a temperature that is slightly higher than the temperature at which they will become saturated for a sufficient amount of time. After that, the crucible is cooled in order to make it possible for the desired substance to crystallise. Crystallisation can get its start through a process called spontaneous nucleation, or it can be sped up with the help of a seed. The amount of solute in the flux drops, which results in a lower temperature at which the solution is saturated. This happens because material is precipitating out of the solution as it does so. As the furnace continues to cool, this process will continue to repeat itself. It will do so either until the solution reaches its melting point or until the reaction is stopped intentionally. It is possible for divergent crystal growth kinetics to occur during the flux method synthesis. This can lead to anomalous grain growth, which is caused by a small number of crystallites growing at the expense of others in the vicinity.

The crystals that are formed using this process frequently have natural facets, which is one of the advantages of the method because it makes it substantially simpler to prepare crys-

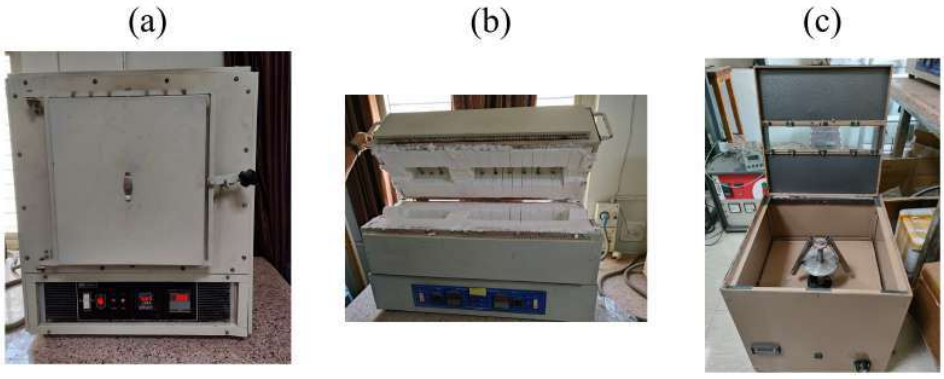

Figure 2.2: Instruments used for single crystal synthesis. (a) Muffle furnace, (b) Two zone furnace for CVT growth and (c) Centrifuge machine which is used for separating the single crystal from the molten flux during the flux growth. (Photograph is taken from our laboratory)

tals for measurement. The majority of flux technique syntheses result in the production of relatively tiny crystals, which is a drawback. Some of the instruments required for single crystal growth are shown in Fig. 2.2

2.1.3 Bridgman technique

The Bridgman–Stockbarger approach, also known as the Bridgman–Stockbarger technique, was named after the physicists Percy Williams Bridgman (1882–1961) of Harvard University and Donald C. Stockbarger (1895–1952) of Massachusetts Institute of Technology. The method incorporates two techniques that are analogous to one another but unique from one another. These techniques are generally utilised for creating boules, which are single-crystal ingots, but they can also be employed for hardening polycrystalline ingots.

The processes require heating polycrystalline material above its melting point and then slowly cooling it from one end of its container, which is where a seed crystal is placed. On the seed material itself, a single crystal with the same crystallographic orientation as the seed material grows, and this crystallisation process continues to occur throughout the length of the container. The procedure can be carried out in either a horizontal or a vertical configuration, and it typically makes use of a revolving crucible or ampoule in order to stir the molten substance.

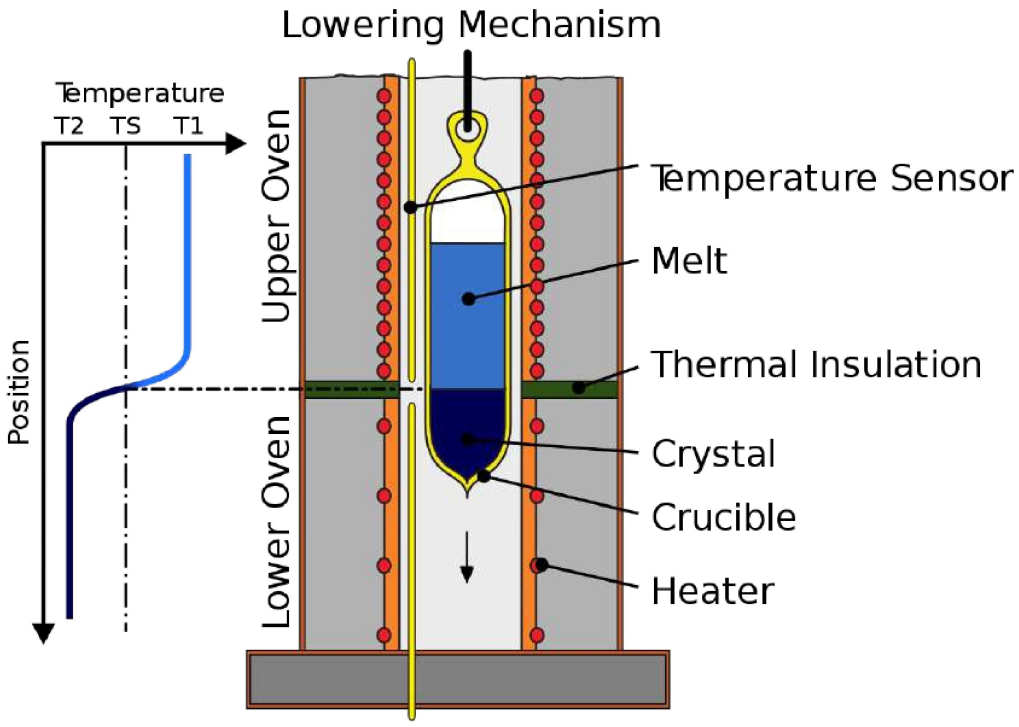

Figure 2.3: The schematic and working principle of the Bridgman technique of single crystal growth. (Photo is taken from the Ref. [34])

When it comes to the production of particular semiconductor crystals, such as gallium arsenide, the Czochralski process is generally considered to be more challenging than the more common Bridgman method. The procedure is capable of producing single-crystal ingots in a dependable manner, although the resulting crystal may or may not have qualities that are consistent throughout. The schematic diagram of the Bridgman technique is shown in Fig. 2.3. The Bridgman furnace in our laboratory is shown in Fig. 2.4. The lab grown single crystal is shown in Fig. 2.5

2.2 Experimental characterization tools

2.2.1 Diffraction of X-rays (XRD)

A diffraction phenomena happens when electromagnetic radiation interacts with a periodic structure. The wavelength of X-rays, which are electromagnetic waves with a very short wavelength of a few angstroms (1 = 0.1 nm), is exceedingly small. The X-ray's

Figure 2.4: The Bridgman single crystal growth furnace. (Photograph taken from our laboratory)

Figure 2.5: The photograph of lab grown single crystal.

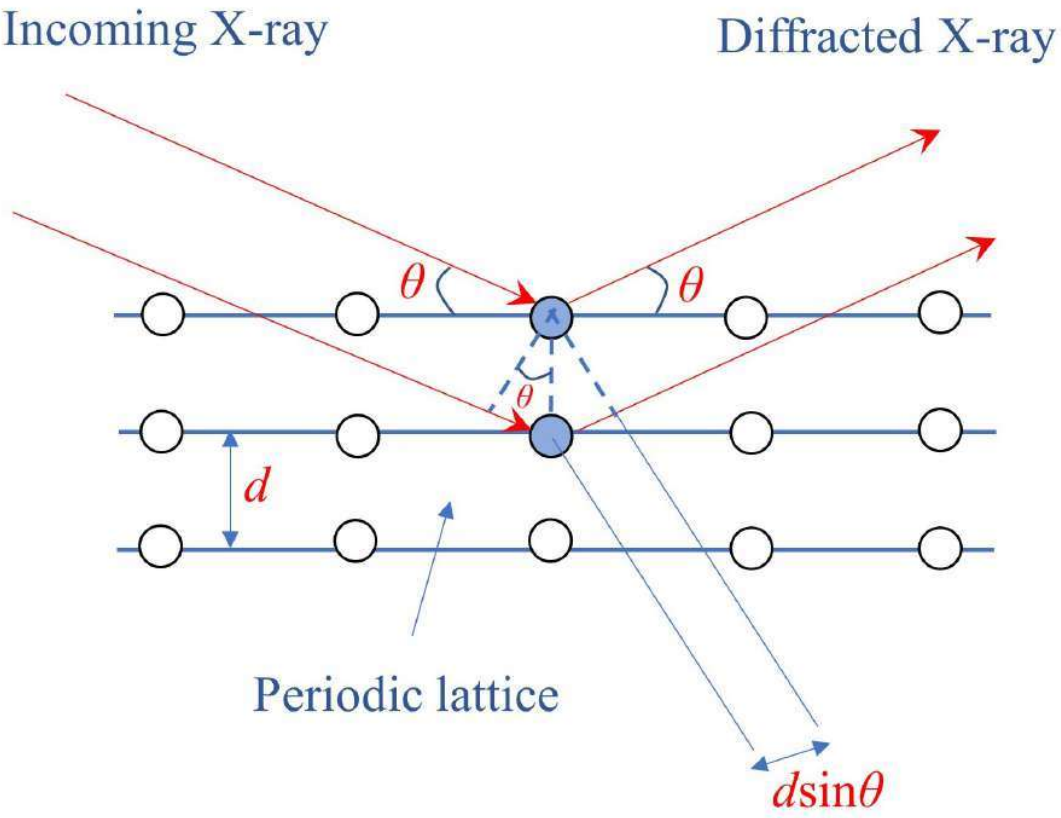

Figure 2.6: Schematic diagram of the X-ray diffraction and the formulation of Bragg's law.

extremely short wavelength indicates its high energy level. The incident X-ray photons interact with the electrons of an atom in the sample when a monochromatic X-ray beam strikes it. Some of the photons are subsequently diffracted away from the direction of their initial incidence. If the size of the barrier is comparable to the wavelength, a phenomenon known as diffraction occurs when the electromagnetic wave bends and creates an obstruction. The interatomic distance in crystalline materials ranges from 1–10 , or the same order of X-ray wavelength. Only when the interference peaks are seen for a specific crystalline solid at specific angles does the constructive interference happen. Atoms are organized regularly in crystals. Assume that Bragg's condition is met when interference caused by diffracted waves from atomic planes. In that instance, measuring the intensity of diffracted waves with a modification in the X-ray incidence angle provides the X-ray diffraction pattern of a given material. The XRD pattern of the sample contains an array of data, including information on the phase of the synthesised sample as well as crystal structure and unit cell dimension. Bragg's law, which was developed by William H. and W. Lawrence Bragg, governs the diffraction of X-rays from crystalline planes[35]. The relationship between the wavelength of X-rays and the angle at which the beam diffracts from the crystalline structure can be understood using Bragg's relation. The relationship may be stated as $2d \sin\theta = n\lambda$. Where λ is the wavelength of X-ray used, n is an integer representing the order of diffraction, d is the inter-planar distance of atoms, and θ is the scattering angle or Bragg's angle. The intensity of diffracted X-ray is recorded as a function of the Bragg angle 2θ. The X-ray diffractometer records the *intensity* vs. 2θ data. The diffractometer has a monochromatic X-ray source with CuK_α radiation (λ=1.5418). The schematic digram of the X-ray diffraction is shown in Fig. 2.6

2.2.2 Laue diffraction pattern

The Laue diffraction study was performed on single crystals. Since Bragg's angle is constant for each set of planes in an immobile crystal when a beam of polychromatic X-ray radiation is impacted onto it, each set diffracts a unique wavelength that satisfies Bragg's condition for the specific values of d and θ. Based on the relative positions of the X-ray

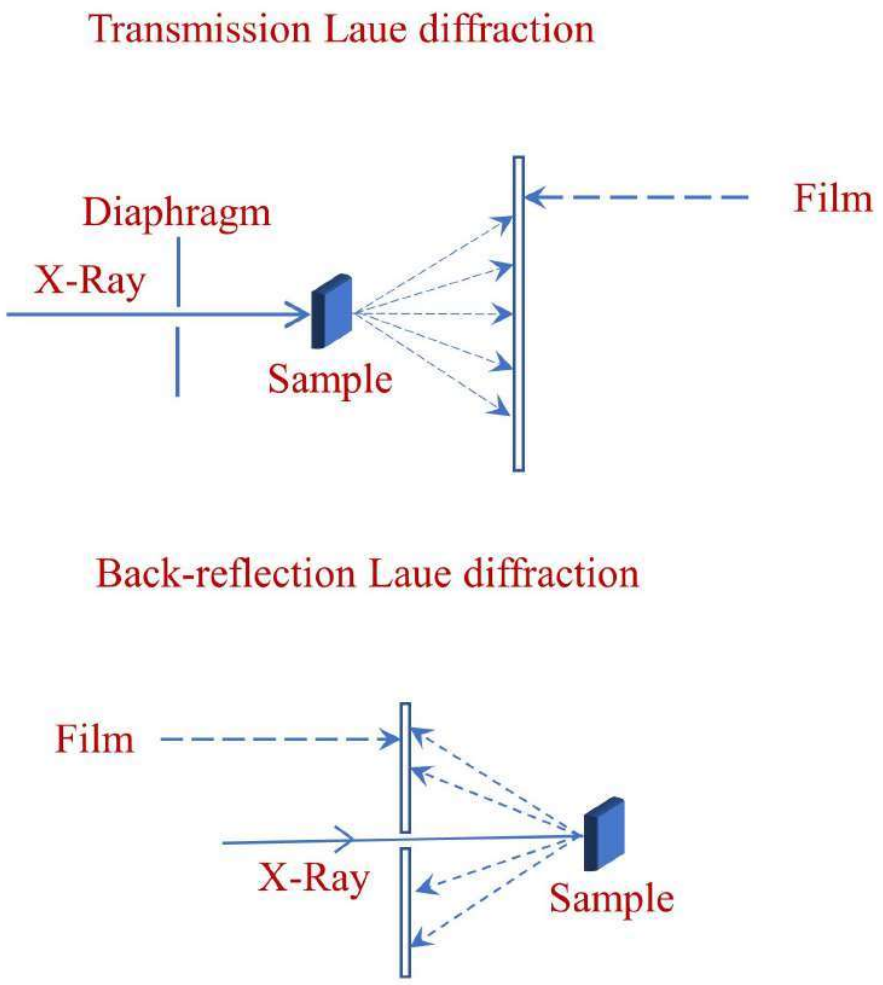

Figure 2.7: Schematic diagram of the Laue diffraction set up. (Upper panel) The transmission method. (Lower panel) The back-reflection method

source and sample, Laue diffraction can be performed in one of two alternative measurement geometries: either the transmission geometry or the back-reflection geometry. Fig. 2.7 depicts both geometries' schematics. The sample is positioned in both geometries so that X-rays incident normally on it. The X-ray beam incident on the sample in the transmission geometry partially passes through the sample and is captured on the photographic film. In contrast, the photographic film in the back-reflection geometry is positioned between the X-ray source and the sample. Photographic film captures the sample's backwards diffracted beams. The diffracted beams create an array of spots for a single crystal sample in both of these geometries.

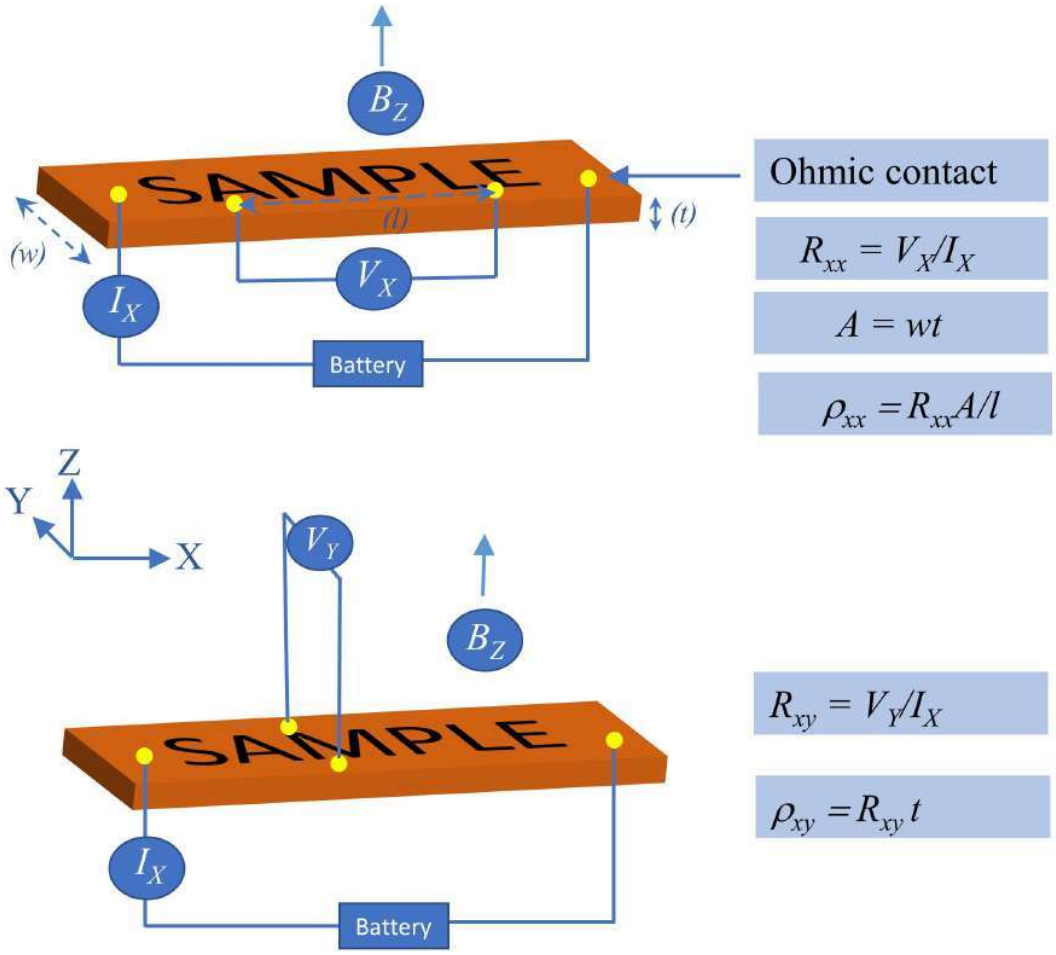

Figure 2.8: The resistivity measurement set up. (Upper panel) The normal resistivity ρ_{xx}. (Lower panel) The Hall resistivity ρ_{xy}.

2.2.3 Electric resistivity (ρ_{xx})

Using a four-probe approach, the resistivity of the synthesised single crystal samples was measured using the Quantum Design Physical Property Measurement system (QD-PPMS). Electrons experience resistance to their motion as they go through the crystal. A potential difference must be applied across the crystal in order to force the electrons to travel against this resistance. Ohm's law states that if current I flows through a crystal with resistance R, voltage V will decrease due to this resistance through the crystal, as shown by the equation $V = IR$. Resistivity (ρ_{xx}) is a quantity that describes the material's intrinsic properties. A particular material's resistivity is influenced by the synthesis method. The distance l between two voltage probes and the cross-sectional area A [thick-

ness (t) $\times$ width (w)] are both proportional to the resistivity of a crystal. In mathematics, it is written as $\rho_{xx} = R_{xx}A/l$. On a uniform rectangular single crystal sample, resistivity measurements were made using a traditional four-probe technique between 2 K and 300 K with applying external magnetic field (called MR) or without applying external magnetic field (called ordinary resistivity), to the sample's surface as shown in the Fig. 2.8.

2.2.4 Hall resistivity (ρ_{xy})

By modifying the connection design as shown in lower panel of Fig. 2.8, the Quantum Design Physical Property Measurement System (QD-PPMS) was also used to measure the Hall resistivity (ρ_{xy}). In this instance, the voltage drop was measured across the sample's opposing surfaces in a direction that was perpendicular to both the external magnetic field (B) and the current (I). A Lorentz force $\mathbf{F} = qv \times \mathbf{B}$ develops on the charge when a particle of charge q moves perpendicular to **B** in a current-carrying conductor. This force is orthogonal to both the direction of the particle motion and the field. So, the transverse voltage or Hall voltage V_Y is measured by applying a constant longitudinal current I across a sample. The precise value of the Hall coefficient ($R_H = 1/nq$) can be obtained from the graph between the measured Hall resistivity ρ_{xy} and the applied magnetic field. The value of R_H can be calculated from the slope of the linear variation of ρ_{xy} as a function of field that is produced. In a sample, a negative value of R_H suggests n-type charge carriers, while a positive value of R_H suggests p-type charge carriers. The value of the Hall voltage, V_Y, is provided by the voltage difference between two opposed surfaces, and the Hall resistance can be calculated as, $R_{xy} = \frac{V_Y A}{Il} = B/net = R_H B/t$ and the Hall resistivity (ρ_{xy}) can be defined as $R_H B = R_{xy} t$. The PPMS instrument used in UGC–DAE Kalpakkam node is shown in Fig. 2.9

2.2.5 Shubnikov–de Haas (SdH) oscillation

The Shubnikov–de Haas effect (SdH) is a macroscopic representation of the inherent quantum mechanical basis of matter. It is an oscillation in the conductivity of a material that happens at low temperatures in the presence of very high magnetic fields. It is frequently

Figure 2.9: 15 T ppms machine for magnetotransport studies

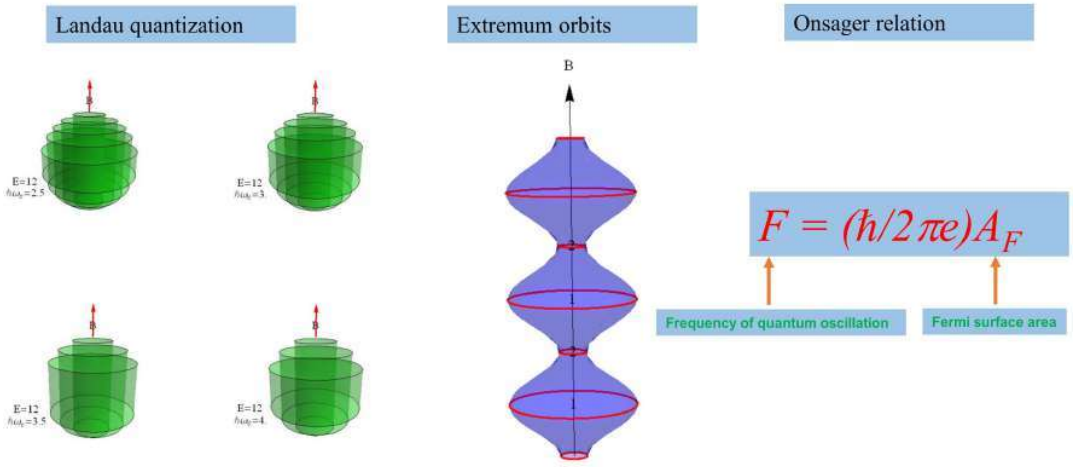

Figure 2.10: Formation of Landau tube on the application of the magnetic field. (Left panel) with the increase of magnetic field, the width of the Landau tubes increase. (Middle panel) The extremum areas of the Landau tube are indicated by the red circle. The frequency of the quantum oscillation is proportional to this area. (c) The mathematical relation between the frequency of oscillation and extremum area of Fermi pockets. (This figure is recreated from the Ref [36])

utilised in the process of determining the effective mass of charge carriers, which includes electrons and holes. Both Wander Johannes de Haas and Lev Shubnikov are honoured with their names being given to this effect. If the temperature is kept low enough and the magnetic field strength is high enough, the free electrons in the conduction band of a metal, semimetal, or narrow band gap semiconductor will operate in a manner similar to that of simple harmonic oscillators. The oscillation period of the simple harmonic oscillators shifts in a manner that is proportionate to the degree to which the magnetic field strength is altered. Landau levels are what make up the energy spectrum that is produced as a result; these levels are divided by the cyclotron energy. The Zeeman energy contributes to an additional division of these Landau levels. With an increase in the magnetic field strength, the cyclotron and Zeeman energies, as well as the number of electron states (eB/h), all rise in a linear fashion within each Landau level. As a consequence of this, the spin-split Landau levels progress to higher energies as the magnetic field strengthens. When a certain energy level travels through the Fermi energy, the population of that level decreases because the electrons then have the opportunity to flow freely as current. Because of this, the transport and thermodynamic properties of the material will oscillate periodically, which will result in an observable oscillation in the material's conductivity. The formation of Landau tubes and the extremum area of the Fermi surface is shown in Fig. 2.10

The oscillation pattern of the resistivity is described by the Lifshitz-Kosevich (LK) formula

$$\Delta R \propto -B^{\lambda} R_T R_{\mathrm{D}} R_S \sin\left[2\pi\left(\frac{F}{B} - \Gamma - \Delta\right)\right] \tag{2.1}$$

where $R_T = \alpha T\mu/B\sinh(\alpha T\mu)$, $R_D = \exp(-\alpha T_D\mu/B)$ and $R_S = \cos(\pi g\mu/2)$. μ is the ratio of the effective cyclotron mass m^* to free electron mass m_0. T_{D} is the Dingle temperature, and $\alpha = (2\pi^2 k_B m_0)/(\hbar e)$. The oscillation phase is described as a sine term with an additional phase factor $\Gamma - \Delta$, in which $\Gamma = \frac{1}{2}$ - $\phi_B/2\pi$ and ϕ_B is the Berry phase. The dimensionality of FS is determined by the phase shift Δ. For 2D FS, Δ = 0. For 3D FS, Δ can take value $\pm$ 1/8 according to the minima and maxima of the FS area. The term λ is also determined by the FS dimensionality. λ can takes value $\frac{1}{2}$ and 0 for 3D

and 2D FS respectively. From the L-K formula, effective mass m^* can be calculated from the fit of the thermal damping factor R_T with the temperature dependent amplitude of the oscillation.

2.2.6 Photoemission Spectroscopy

The well-known experiment conducted by Heinrich Hertz in 1887 serves as the beginning of the history of photoemission[37]. He discovered that a negative charge may be extracted from a material's surface by putting an ultraviolet light on it. Albert Einstein then confirmed the quantum nature of light and clarified the photoemission process in 1905[38]. One of the most useful technologies today for figuring out a material's electronic structure is photoelectron spectroscopy. The majority of the macroscopic properties displayed by materials are derived from the microscopic electron dynamics close to the E_{F}. Therefore, in order to analyse these extremely low-energy electronic states, very high-resolution analyzers are needed. Scienta created an electron analyzer with an energy resolution of 20–40 meV in the middle of the 1990s; it has now been upgraded to 5 meV. A vacuum ultraviolet laser-based photoemission spectrometer with extremely fine resolution has also been created recently. Numerous odd features, like TSS, topological Fermi arcs, and other phenomena, are experimentally confirmed because of these technological advancements. When a photon with energy $E = h\nu$ strikes a material's surface and its energy is high enough, it can free an electron from its bound state inside the material. The extracted electron is known as a photoelectron, and an analyzer can be used to determine its kinetic energy (E_{KE}). The photoelectron's E_{KE} is stated as,

$$E_{KE} = h\nu - (E_{BE} - W_{\phi}) \tag{2.2}$$

Where, E_{BE} is the binding energy of electron and W_{ϕ} is the work function of material. The momentum (**k**) of the photoelectron can also be estimated from the E_{KE} as,

$$\mid \mathbf{k} \mid = \sqrt{2m_e E_{KE}}/\hbar \tag{2.3}$$

2.2.7 Angle-resolved photoemission spectroscopy (ARPES)

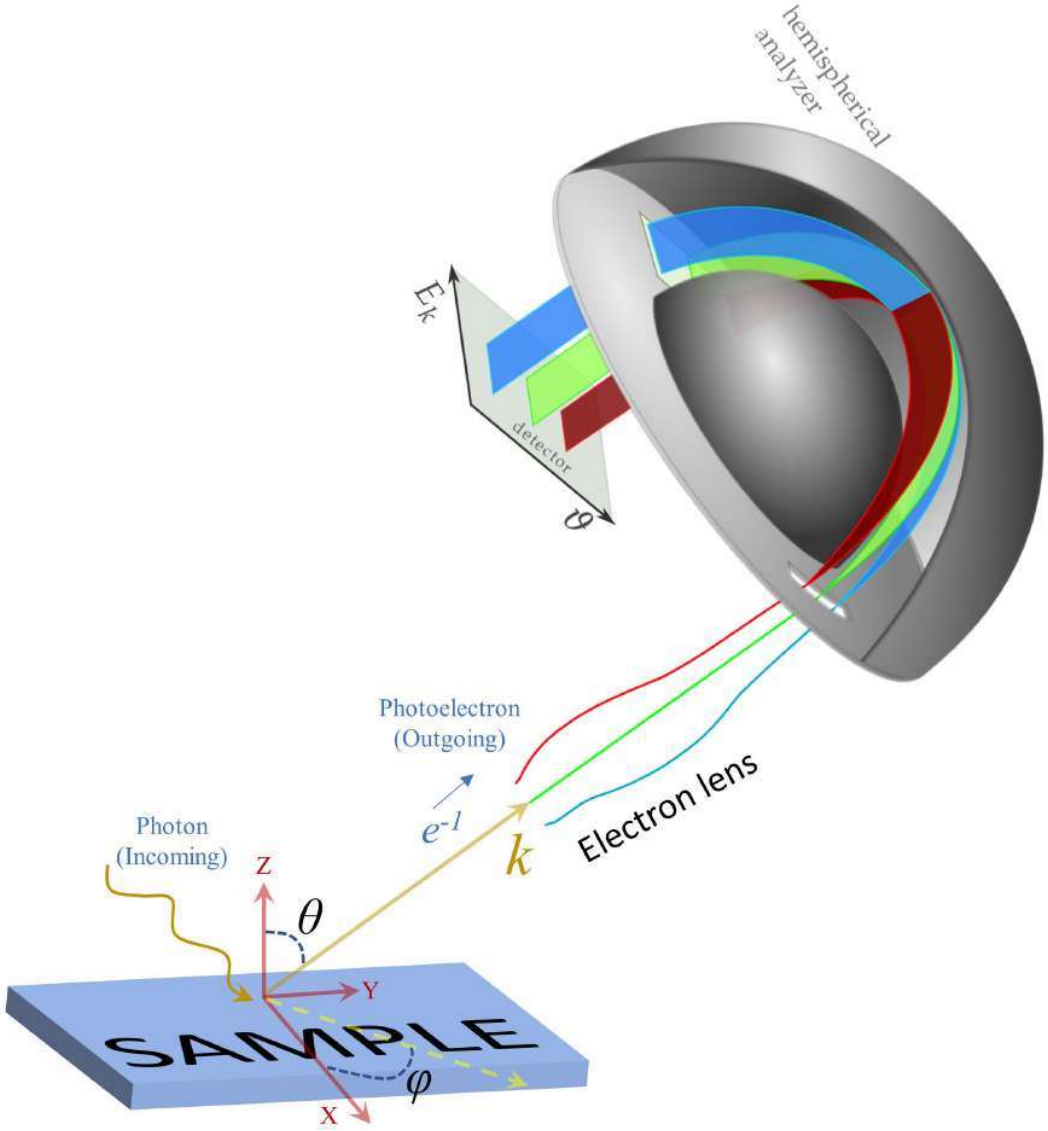

Figure 2.11: Schematic diagram of angled-resolved photo-emission spectroscopy (The photo of analyzer is taken from Ref. [39])

The direct visualization of the electronic structure in the materials is made possible by the valuable technology known as ARPES. It also makes use of the well-known photoelectric effect in its work. The energy or momentum of photoemitted electrons from the material can be examined in light of the relevant information, which can then be compared with the theoretical simulation for the material for a complete understanding of the physics of the material.. The photoemission process's energy and momentum (parallel component) conservation makes this possible. The ARPES experiment is conducted in a UHV set-

ting, much like the XPS, with a monochromatic incident photon beam that often comes from a synchrotron source. ARPES measurements for TIs provide a clear view of the bulk electronic band structure and TSS. As a result, the presence of the bulk band gap in the materials as well as the conduction band, valance band, and TSS, are all easily discernible. In order to examine the impact of magnetic doping on the TSS in TIs, ARPES is a helpful method. Since the TSS in TIs is shielded by the TRS, nonmagnetic impurities have no effect on them, and as a result, there is no band gap at the DP. In contrast, the doping of magnetic impurities causes the TRS to be broken, which results in a gap opening at the DP. Since the photoemitted electron's energy and momentum are conserved, and since the momentum of the ejected electron is correlated with its measured angle, we can calculate the photoemitted electron's wavenumber as

$$k_x = \frac{\sqrt{2m_e E_{KE}}}{\hbar} \sin\theta \sin\phi \tag{2.4}$$

$$k_y = \frac{\sqrt{2m_e E_{KE}}}{\hbar} \sin\theta \cos\phi \tag{2.5}$$

$$k_z = \frac{\sqrt{2m_e E_{KE}}}{\hbar} \cos\theta \tag{2.6}$$

Therefore, one can comprehensively map the $E(\mathbf{k})$ dispersion relation of the electrons in the BZ from the above information. All single crystals are not appropriate for ARPES assessment since this technique often involves the cleaving of single crystals to provide a clean, uniform surface. Therefore, the ARPES measurement becomes challenging if single crystals are unavailable or difficult to cleave. The schematic diagram of electrons' energy-momentum mapping is shown in Fig. 2.11, where emitted electrons (photoelectrons) passed through the hemispherical analyzer before falling on a 2D position sensitive detector. During the traversal of the photoelectron through the hemispherical analyzer the electrons are discriminated on the basis of their energy and momentum; and thus the $E-k$ plot is created. The actual beamline ARPES machine used in 'Hiroshima Synchrotron Radiation Center' is shown in Fig. 2.12

Figure 2.12: The beamline ARPES machine. (Photograph taken from the 'Hiroshima Synchrotron Radiation Center')

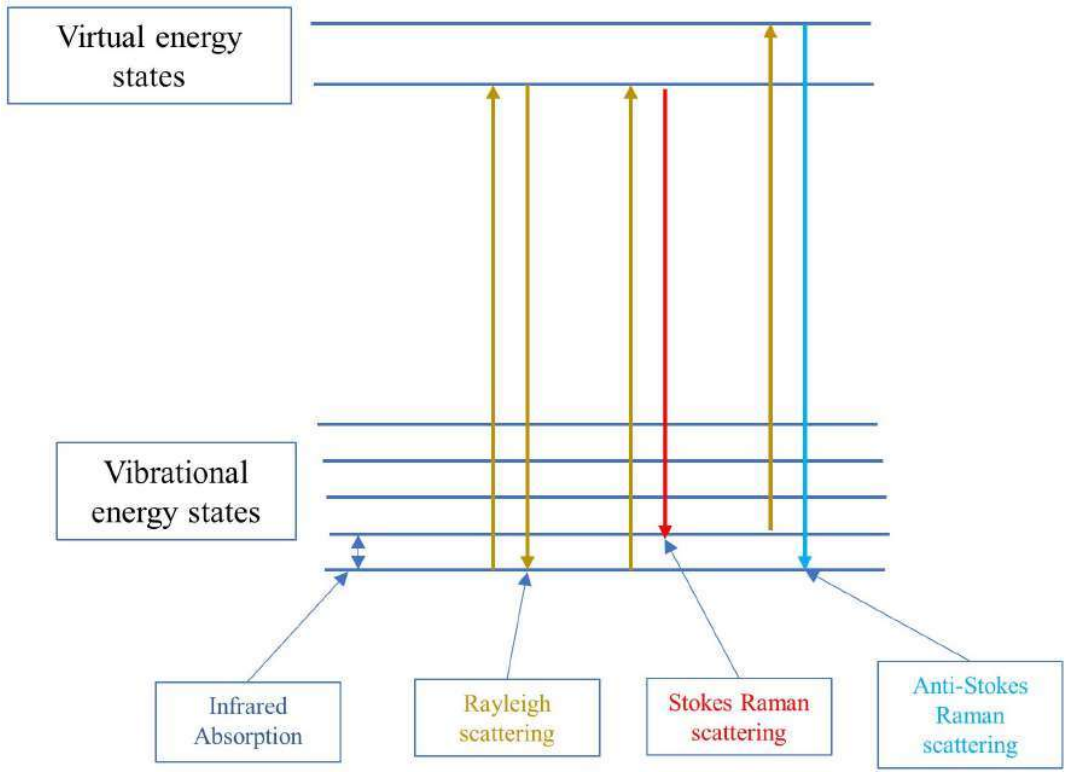

Figure 2.13: The schematic diagram of the Raman effect, (Yellow) Incident ray and Rayleigh scattering, (Red) Stokes Raman scattering, (Indigo) Anti-Stokes Raman scattering.

2.2.8 Raman effect

In 1928, C. V. Raman discovered the Raman effect, which describes the inelastic scattering of light by a substance. Raman effect was named after the scientist who discovered it. The majority of the photons that are dispersed by a material when it is lit, scatter elastically. This phenomenon is known as Rayleigh scattering, in which the scattered frequency is the same as the initial one. On the other hand, a very small of incident light scatter inelastically, which is referred to as Raman scattering, and this results in the final frequency being either greater or lower than the incident frequency. These photons that have been inelastically scattered carry the energy of the distinctive molecular/lattice vibrations that are present in the sample, which results in a shift in the frequency of those vibrations. The following is an example of how the hypothesis of the microscopic origin for the Raman effect might be created.

Interaction of the material with the incident photon causes either the creation/destruction

of one/multiple phonons of the lattice vibrations. Let us assume a photon with angular frequency ω_i is incident on the material's surface. During this process, the increase (anti-Stokes component) or decrease (Stokes component) in the frequency (ω_s) of the scattered photon ($\omega_s = \omega_i \pm \omega$) compensates for the energy that is either lost or gained by the lattice. If we take into account the first-order Raman effect, we will see that the scattering process results in either the creation or destruction of a single phonon.

It is important to take note that this process involves three stages: first, a photon (ω_i) is absorbed, then an optic phonon (ω) is generated, and finally, a photon (ω_s) is emitted. When the process of scattering first begins, we can fairly assume the sample to be in its ground state. At the conclusion of the scattering event, it reverts back to the ground state that it was in. Excitation of electron-hole pairs is required for the existence of the virtual intermediate states. The scattering signals will either appear on the low energy side or the high energy side of the spectrum, depending on whether the incident photons interact with a molecule when it is in its vibrational ground state or when it is in its excited state. A higher energy state is reached by the scatterer as a result of the Stokes scattering. On the other hand, anti-Stokes emission can only take place if the scatterer, which is already in an excited state, degenerates into a lower energy state. Due to the fact that they are produced by the same upper and lower energy levels, the Stokes and anti-Stokes Raman modes both exist in a symmetrical pattern around the Rayleigh line. However, in comparison to the Stokes lines, the anti-Stokes lines have a far lower intensity. This is due to the fact that the number of molecules in an excited vibrational state is extremely low. In modern times, Raman spectroscopy has developed into a well-liked, non-destructive, and potent method for analysing the lattice dynamics and structural symmetries of a system. The Horiba LabRam HR evolution spectrometer was used to conduct a temperature-dependent Raman investigation. The sample was exposed to a He-Ne laser at a wavelength of 633 nm. When taking Raman measurements at different temperatures, the sample was chilled with liquid nitrogen from 300 to 100 K before the measurements were taken. The schematic diagram of the incident ray, Rayleigh scattering, Stokes Raman scattering, anti-Stokes Raman scattering and the vibrational energy state are shown in Fig. 2.13